Ground-based remote sensing of aerosol optical properties and their radiative impacts in the PRD region of China

Boru Mai[1], Xuejiao Deng[1], Zhanqing Li[2,3], Jianjun Liu[3], Xiangao Xia[4], Huizheng Che[5], Xia Liu[6], Fei Li [1], Yu Zou[1], Maureen Cribb[3]

[1]Institute of Tropical and Marine Meteorology/Guangdong Provincial Key Laboratory of Regional Numerical Weather Prediction, China Meteorological Administration, Guangzhou China

[2] State Key Laboratory of Earth Surface Processes and Resource Ecology and College of Global Change and Earth System Science, Beijing Normal University, 100875, Beijing, China

[3] ESSIC and Department of Atmospheric and Oceanic Science, University of Maryland, College Park, Maryland, USA

[4] LAGEO, Institute of Atmospheric Physics, CAS, Beijing, China

[5] Chinese Academy of Meteorological Sciences, Beijing, China

[6] Guangzhou Meteorological Observatory, Guangzhou China

Correspondence to: Zhanqing Li, zli@atmos.umd.edu

Abstract Aerosol direct radiative effects on surface irradiance were examined using seven years of ground-based spectral radiation data collected at Panyu, the main atmospheric composition monitoring station in the Pearl River Delta (PRD) region of China. Aerosol optical properties were derived from sunphotometer measurements, which were then used as input to a radiative transfer model to calculate broadband radiation. In the dry season (October to the following February), the mean aerosol optical depth (AOD) at 550 nm was 0.535. More than 60% of AOD values ranged from 0.2 to 0.6. The mean value of the Angstrom exponent (AE) calculated from AOD retrievals at 440 nm and 870 nm was 1.31, with AE greater than 1.2 in 84.7% of the cases. The mean single-scattering albedo (SSA) at 440 nm was 0.87. About 84.82% of SSA values were between 0.8-0.92. Because few dust events take place in the PRD region, the coarse mode of aerosols was negligible. However, the proportion of fine-mode, weakly absorbing particles was about 9.52%. The magnitudes of AE, SSA, and AOD for this subset of data were 1.30, 0.96, and 0.65, respectively. About 90% of aerosols were dominated by fine-mode, strongly absorbing particles with AE, SSA, and AOD equal to 1.35, 0.86, and 0.52, respectively. Because of the strong absorption, the overall aerosol direct radiative effect was to heat the atmosphere and cool the surface. The annual mean shortwave direct radiation forcing at the surface, inside the atmosphere, and at the top of atmosphere was -33.51±8.41, 27.29±7.19, and -6.22±2.22 $W \cdot m^{-2}$, respectively. Strongly absorbing aerosols not only changed the amount of global shortwave radiation reaching the surface, but also dramatically changed the proportion of diffuse to direct radiation at the surface. The annual mean reduction in surface global and direct radiation due to aerosols was -37.50±9.43 $W \cdot m^{-2}$ and -81.89±18.42 $W \cdot m^{-2}$, respectively. The presence of

aerosols resulted in 44.38±9.49 $W \cdot m^{-2}$ more diffuse radiation reaching the earth's surface. Due to the significant radiative impacts of fine-mode, strongly absorbing particles, the properties of carbonaceous aerosols in the PRD region and their impacts on regional climate change should be further studied.

Key Points:

- The aerosol properties of the PRD region in China are determined.
- The aerosol radiative forcing in the PRD is derived for the first time over a long period of time.
- Providing a key constraint for model simulation of regional anthropogenic aerosol effects.

1. Introduction

Aerosols have been recognized as a major factor in determining global and regional climate change [*IPCC*, 2007]. They play crucial roles in not only solar and thermal radiative transfer in the atmosphere [*Kosmopoulos et al.*, 2008], but also in the hydrologic cycle [*Rosenfeld et al.*, 2008; *Clarke and Kapustin*, 2010], the carbon cycle [*Chameides et al.*, 1999], and some important environmental issues such as acid rain and tropospheric ozone pollution [*Wang*, 1999]. The spatial and temporal variations in aerosols highlight the need to quantify aerosol radiative properties and forcing on a regional scale. However, limited information on aerosol optical properties and radiative forcing (ARF) are still major uncertainties [*Guan et al.*, 2010] because of differing aerosol types, compositions, and their generally large spatio-temporal variations. This is especially so in the vast territory of China.

Aerosol radiative impacts are strongly dependent on its optical properties. To better understand the direct effect of aerosols on the surface energy budget and their associated impacts on climate, some key parameters such as aerosol optical depth (AOD), the Angstrom exponent (AE), single-scattering albedo (SSA), and the asymmetry factor (ASY) are needed. The latter two parameters are difficult to retrieve from conventional satellite observations [*Kaufman et al.*, 2002a, 2002b; *Li et al.*, 2009]. Sunphotometer, lidar, aircraft, and satellite observations have been used to analyze the spatial and temporal characteristics of the above parameters [*Xia et al.*, 2007a; *Guan et al.*, 2010; *Liu et al.*, 2012; *Che et al.*, 2014] and to estimate aerosol direct radiative forcing [ADRF; *Li et al.*, 2010; *Alam et al.*, 2011; *Choi and Chung*, 2014]. The magnitude of the global ADRF (due to absorption and scattering) has been estimated to range from -0.85 $W \cdot m^{-2}$ to -0.15 $W \cdot m^{-2}$ [*Myhre et al.*, 2013]. Based upon data from 25 observation sites spread across China, the ARF estimate over China shows that aerosols have little impact on the atmosphere−surface system, but substantially warm up the atmosphere at the expense of cooling the surface [*Li et al.*, 2010]. Heavy aerosol loading and strong aerosol absorption over northern and southeastern China lead to substantial reductions in direct and global shortwave irradiances at the surface while the instantaneous aerosol direct forcing at the top of the atmosphere (TOA) is close to zero [*Xia et al.*, 2007a; *Liu et al.*, 2012].

Until now, little knowledge about aerosol radiative properties and forcing in the Pearl River Delta (PRD) region through ground-based remote sensing has been gained. This region is the largest and most important economic zone in China where the open-door policy and drastic economic reform took place in 1980s. Due to the rapid growth of industrialization and urbanization over the past decades, the amounts and rates of emission of atmospheric pollutants have increased dramatically. As a result, aerosols have become the most serious of atmospheric pollutants in the region [*Deng et al.*, 2006; *Wu et al.*, 2008]. A recent study [*Deng et al.*, 2011] has shown that the probability that AOD at 550 nm is ≥ 0.6 and AOD at 340 nm is ≥ 1.0 is 47% and 55%, respectively, during the dry season (October to January). Under current pollution conditions in the region, more than half of the surface radiation, especially at ultraviolet wavelengths, has been reduced by aerosols [*Deng et al.*, 2011]. Part of this reduction is driven by industry that consumes a substantial amount of fossil fuel and coal in this region and releases more absorbing soot and organic aerosols into the atmosphere [*Cao*, 2003, 2004; *Cheng et al.*, 2008; *Wu et al.*, 2009]. Since 2006, extensive measurements of aerosol optical, physical, and chemical properties over the PRD region have been made.

In this paper, sunphotometer data from this region are used for the first time to: (1) analyze the frequency and monthly distributions of AOD, SSA, AE, and relative humidity (RH), (2) classify major aerosol types using AE and the scattering co-albedo (ω), and (3) examine ADRF over the region. Section 2 describes the observational site, the instrumentation at the site, and the methodology used in the study. Section 3 presents results and discussion. Conclusions are given in Section 4.

2. Data and methodology

2.1 Observational site and instrumentation

Panyu (113.35°E, 23°N, 141 m above sea level) is located in the central part of the PRD region (Fig. 1). It is the main site of the atmospheric composition network run by the Guangdong Provincial Meteorological Bureau. Since 2011, this site has become part of the China Aerosol Remote Sensing Network (CARSNET). Measurements made at Panyu represent the basic characteristics of atmospheric composition in the PRD region [*Wu et al.*, 2009].

Characterization of atmospheric aerosols is done using a sunphotometer (CIMEL Électronique, Paris, France). This instrument makes direct sun measurements every 15 min with a 1.2° full field-of-view at 1020, 870P1, 670, 440, 870P2, 870, 936, and 870P3 nm (P indicates a polarized filter). The full-width at half-maximum of each interference filter is 10 nm. Measurements at 1020, 870, 670, and 440 nm are used to retrieve AOD and measurements at 936 nm quantify the total precipitable water vapor. The raw AOD is cloud-screened according to the method of Smirnov et al. [2000] with an uncertainty of < ±0.01 for wavelengths > 440 nm [*Eck et al.*, 1999].

The CIMEL sunphotometer also measures sky radiances under almucantar and principal plane scenarios at 440, 670, 870 and 1020 nm following the optical air mass protocol described by *Holben et al.* [1998]. Aerosol inversion algorithms and software (SKYRAD.pack version 4.2) are used to retrieve aerosol optical and physical properties from sky radiances. Aerosol particle parameters such as SSA, the refractive index, and the particle volume size distribution are obtained by this technique [*Nakajima et al.*, 1996]. Calibration of the sunphotometer was performed by CARSNET following the protocol developed by the Aerosol Robotic Network (AERONET). Details about the inter-comparison calibration and sphere calibration carried out at the Chinese Academy of Meteorological Sciences are given by *Che et al.* [2009] and *Tao et al.* [2014].

2.2 Methodology

2.2.1 Retrievals of AOD, ω, and AE

The retrieval of columnar aerosol radiative properties from sky radiances requires an accurate correction for the effects of multiple scattering and for the contribution of light reflected from the earth's surface and scattered downward in the atmosphere [*Valenzuela et al.*, 2012]. The SKYRAD.pack version 4.2 software [*Nakajima et al.*, 1996], which is commonly used to retrieve aerosol optical and radiative parameters [e.g., *Kim et al.*, 2005; *Liu et al.*, 2008; *Che et al.*, 2008; *Khatri et al.*, 2014; *Wang et al.*, 2014], was used to calculate AOD and SSA by using a radiative transfer code as well as linear and nonlinear inversion schemes. Additional input parameters for the SKYRAD.pack included ozone data from the Atmospheric Infrared Sounder, and surface albedo from the Moderate Resolution Imaging Spectroradiometer (MODIS) Level 2 Collection 5 spectral surface reflectance product. The parameter ω describes the loss of photons to absorption, which is useful in identifying particle composition, especially carbonaceous particles [*Corrigan et al.*, 2006]. Here, ω is expressed as

$$\omega(\lambda) = 1 - SSA(\lambda), \tag{1}$$

where λ is the wavelength.

The AE is a good indicator of the size of particles and is given by the following equation:

$$AE = -\frac{\ln[\frac{AOD(\lambda_1)}{AOD(\lambda_2)}]}{\ln[\frac{\lambda_1}{\lambda_2}]}, \qquad (2)$$

where λ_1 and λ_2 are the two wavelengths chosen to calculate AE. The wavelength pair of 440 nm/870 nm is used in this study. AE can range from negative values to greater than 1 [*Eck et al.*, 1999; *Gobbi et al.*, 2007], depending on the particle size.

2.2.2 Radiative forcing and radiative forcing efficiency

Radiative fluxes and aerosol direct radiative effects of total, diffuse, and direct shortwave irradiances in the broadband spectral range (0.25-4.00 μm) are calculated using the Santa Barbara DISORT Atmospheric Radiative Transfer (SBDART) tool [*Ricchiazzi et al.*, 1998]. Previous studies have shown that SBDART simulations of downwelling broadband fluxes at the surface agree well with ground-based measurements and that simulated upwelling fluxes at the TOA are compatible with Clouds and Earth's Radiant Energy System satellite retrievals in terms of absolute differences [*Xia et al.*, 2007a; *Li et al.*, 2010]. SBDART simulations and measurements of broadband irradiance agree to within 3% [*Halthore et al.*, 2005]. This model has been used to estimate aerosol radiation forcing in China [*Xia et al.*, 2007c, 2007d; *Liu et al.*, 2007; *Li et al.*, 2010].

The AOD, SSA, AE, and ASY at four AERONET wavelengths (i.e., 440, 675, 870, and 1020 nm) have been used to interpolate and extrapolate into the spectral divisions of the SBDART model [*Xia et al.*, 2007a, 2007b]. The value for the ASY from the AERONET site in Hong Kong was used here and assumed to be constant. Other input parameters for the SBDART model include ozone data from the Atmospheric Infrared Sounder, water vapor from the MODIS atmospheric profiles product, and surface albedo from the MODIS Level 2 Collection 5 spectral surface reflectance product [*Liu et al.*, 2012].

ADRF is commonly used to quantify the direct effect of aerosols on the atmospheric energy budget. The SBDART model was run twice to simulate shortwave irradiances with and without aerosol particles under cloud-free conditions, and then used to determine ADRF at the surface (F_{SFC}) and at the TOA (F_{TOA}). The aerosol radiative forcing within the atmosphere (F_{ATM}) is defined as the difference between F_{TOA} and F_{SFC}. The definition of diurnal mean radiative forcing is often given as

$$dF = \frac{1}{24}\int F(t)dt \quad , \qquad (3)$$

where *F(t)* represents instantaneous radiative forcing values. The combined error caused by uncertainties in main input parameters, including AOD, AE, SSA, ASY, surface reflectance, and ozone amounts, is 8.76±3.44 $W \cdot m^{-2}$ [*Li et al.*, 2010].

2.2.3 Data description

The data derived from the sky radiation algorithm was used to analyze AOD, SSA, and AE at a temporal resolution of 30 min. The temporal resolution of ADRF is the same as that of the aerosol property parameters. The sunphotometer collected 1219 inversion measurements from

January 2006 to December 2012. However, observations were not continuous due to instrument calibration and maintenance [*Zhu et al.*, 2014]. In addition, the PRD region is typically cloudy and rainy during the wet seasons (spring and summer), which greatly influences instrument observations and data inversions. For this reason, this study focuses on the dry season (October to the following February). Table 1 summarizes the number of days in each of these months with inversion data available and the total number of data points in each of these months.

3. Results and discussion

3.1 Aerosol optical properties

Figure 2 shows the frequency distributions of AOD at 550 nm, AE, SSA at 440 nm, and RH over the PRD region. The annual mean RH was 57.53%. The most frequent value of RH ranged from 50-60%, typical of the dry season in the PRD region (Fig. 2d).

AOD ranged from ~0.1-1.3 (Fig. 2a). More than 60% of AOD values were between 0.2 and 0.6, with a maximum frequency (19.13%) at AOD equal to 0.3. The proportions of AOD values below and above this AOD range were 23.65% and 16.09%, respectively.

The AE is a good indicator of particle size. Values of AE < 0.75 indicate mainly coarse-mode particles and values of AE > 1.2 indicate mainly fine-mode particles. Values of AE between 0.75 and 1.2 suggest complicated aerosol modes [*Eck et al.*, 2005; *Yang et al.*, 2011]. Figure 2b shows that AE varied from 0.7 to 1.6. About 15.4% of the particles had AE < 1.2 and up to 84.7% of the particles had AE > 1.2, indicating that aerosols in the PRD region were of the fine-mode variety.

Values for SSA ranged from 0.58 to 0.98 with the most frequent value equal to ~0.88 and the mean value equal to 0.81. About 84.8% of SSA values ranged from 0.8 to 0.92, suggesting that the aerosols were strongly absorbing.

Figure 3 shows notched box whisker plots of monthly AOD at 550 nm, AE, SSA at 440 nm, and RH over the PRD region. From October to February, AOD varied from 0.47 to 0.75, with a maximum in February and a minimum in December (Fig. 3a). The annual mean value was 0.535, which is relatively less than values of AOD reported at sites in eastern China like Lin'an [*Che et al.*, 2009] and Taihu [*Liu et al.*, 2012]. This is likely because only the dry season was considered here.

Monthly changes in AE were not apparent (Fig. 3b). The magnitude of AE ranged from 1.31 to 1.38 and was relatively higher in February and October and lower in December. The mean value of AE was 1.33, which is higher than the values retrieved at Xinglong [*Zhu et al.*, 2013], and in northern [*Xia et al.*, 2007b] and northeastern [*Xin et al.*, 2011] China. Local pollutants and the products of their photochemical reactions are the prime sources of aerosols in the PRD region, while the other sites mentioned are in northern China, which is more susceptible to coarse-mode mineral dust. As a result, the particles have fine-mode properties which reach their maximum values in February. The high AOD and AE in February may be related to the high water content in the atmosphere during that month (Fig. 3d) and to pollutants advected in from cities around the PRD region.

The mean value of SSA was 0.87 (Fig. 3c), which is lower than the values reported at Xianghe [*Li et al.*, 2007] and Xinglong [*Zhu et al.*, 2014]. This suggests that aerosols are strongly absorbing in the PRD region. There was little month-by-month change in SSA, but relatively higher values are seen in October and February. This could be due to the presence of water-soluble aerosols at higher RH levels, resulting in fine-mode particle growth and an increase in the light scattering coefficient [*Kotchenruther and Hobbs*, 1998]. The RH level was lower in October (Fig. 3d), but AOD, AE, and SSA values were higher. This may be related to the stronger solar radiation present in October which can activate photochemical reactions and yield more secondary organic aerosols [*Liu et al.*, 2009; *Lee et al.*, 2010].

3.2 Aerosol classification using AE and ω

The wavelength dependence of ω provides more information about the physico-chemical properties of aerosol types and AE provides information about particle size [*Logan et al.*, 2013]. Therefore, these two parameters were combined to classify aerosol types in the PRD region.

As done by *Logan et al.* (2013), ω = 0.07 was chosen as the demarcation line between strongly and weakly absorbing aerosols, and AE = 0.75 was chosen as the demarcation line between fine-mode and coarse-mode particles. Four regions are thus defined: Region I where fine-mode, weakly absorbing particles dominate; Region II where fine-mode, strongly absorbing particles dominate; Region III where coarse-mode, strongly absorbing mineral dust particles dominate; and Region IV where coarse-mode, weakly absorbing particles dominate, e.g., desert aerosols.

Figure 4 shows mean classification results for the months of October to February of the years 2006-2012. About 9.5% of all data points fell in Region I, i.e., the region representing fine-mode, weakly absorbing particles. There was a maximum in October (14.68%), a minimum in January (6.16%), and equal proportions (12%) in November and February. AOD (equal to 0.65) was significantly positively correlated with the aerosol proportions in this region. Up to 90% of particles fell in region II, with a maximum proportion of 93% in January and a minimum proportion of 83.49% in October. In addition, the majority of data points were centered on ω values between 0.07 and 0.17, and AE values between 1.2 and 1.5. As in region I, the proportion in November and February was similar (about 87%). Because few dust events take place in the PRD region, the number of data points in the coarse-mode regions (III and IV) was negligible.

Overall, fine-mode, strongly absorbing aerosol particles were dominant in the study area with mean AOD, AE, and SSA values equal to 0.52, 1.35, and 0.86. Given the location of Panyu, pollutants at the site were likely a combination of carbon aerosols (e.g., organic and black carbon) or mixtures of sulfate, nitrite, and carbon aerosols generated by vehicles and stoves [*Andreae et al.*, 2008; *Zheng et al.*, 2011; *Wang et al.*, 2012]. Compared to region II, aerosols in region I had a higher AOD (0.65) and larger particle size (AE = 1.30). The AOD was significantly influenced by the proportion of particle amount (r = 0.92).

3.3 Diurnal radiative effects

In the PRD region, high aerosol loading prevails all year round with an annual mean AOD equal to 0.54. As a result, aerosols are expected to seriously impact irradiances travelling between the atmosphere and the earth's surface. They are also expected to impact the partitioning between the direct and diffuse components of the surface irradiance. Data from region II are analyzed here because this region contains the largest number of data points.

ADRF varies significantly in different regions and at different time scales [*Yu et al.*, 2006; *Xia et al.*, 2007a; *Li et al.*, 2010]. Global mean values of F_{SFC}, F_{TOA}, and F_{ATM} from observations over land are -11.9, -4.9, and 7.0 $W \cdot m^{-2}$, respectively, and from modeling are -7.6, -3.0, and 4.0 $W \cdot m^{-2}$, respectively [*Yu et al.*, 2006, 2009]. *Li et al.* [2010] found that F_{SFC}, F_{TOA}, and F_{ATM} was -15.7 ±9.0, 0.3 ± 1.6, and 16.0 ± 9.2 $W \cdot m^{-2}$, respectively, over China, and that F_{SFC} could reach -32.8 $W \cdot m^{-2}$ in northern China.

Figure 5 shows the monthly mean diurnal ADRF in the PRD region. The annual mean F_{SFC}, F_{ATM}, and F_{TOA} was -33.51±8.41, 27.29±7.19, and -6.22±2.22 $W \cdot m^{-2}$, respectively. The large negative F_{SFC} and positive F_{ATM} implies strong cooling at the surface and strong warming in the atmosphere, which were likely induced by the large values of AOD and small values of SSA [*Lee et al.*, 2007; *Zhao and Li*, 2007]. The largest monthly values are seen in February when F_{SFC} and F_{ATM} reach -42.88 and 36.06 $W \cdot m^{-2}$, respectively. *Li et al.* [2010] reported that the largest negative F_{SFC} (-20 to -32 $W \cdot m^{-2}$) and positive F_{ATM} (20-40 $W \cdot m^{-2}$) were found over east China in 2005, and the second largest negative F_{SFC} (-20 to -30 $W \cdot m^{-2}$) and positive F_{ATM} (20-30 $W \cdot m^{-2}$) were found over the PRD region. The F_{TOA} ranged from 0-10 $W \cdot m^{-2}$. *Liu et al.* [2012] found that at Taihu, annual mean F_{SFC}, F_{TOA}, and F_{ATM} were -34.8± 9.1, -8.2 ± 4.8, and 26.7 ± 9.4 $W \cdot m^{-2}$, respectively. The magnitude of mean F_{SFC} in this study is similar to that reported in east China and at Taihu. If the same time scale is considered (October to the following February), the F_{SFC} in the PRD region was stronger. Given that this study is based on data collected a few years after 2005, this suggests that anthropogenic aerosol contamination has become a more serious problem in the region and has changed the energy balance at the earth's surface there.

The aerosol radiative forcing efficiency (ADRFE), defined as forcing per unit AOD, is an indicator of the radiative forcing potential of a given type of composite aerosol [*Pathak et al.*, 2010]. The annual mean ADRFE in this study was -68.25±17.18 Wm^{-2} τ^{-1} at the surface, -12.67±4.52 Wm^{-2} τ^{-1} at the TOA, and 55.58±14.64 Wm^{-2} τ^{-1} within the atmosphere (Fig. 6). These values are significantly higher than those reported by *Li et al.* [2010] over China (-35.1 Wm^{-2} τ^{-1}, -0.5 Wm^{-2} τ^{-1}, and 34.5 Wm^{-2} τ^{-1} at the surface, the TOA, and within the atmosphere, respectively). The ADRFE at the surface was higher than that estimated for Xianghe (-65.4±4.7 Wm^{-2} τ^{-1}), Taihu (-54.4±5.3 Wm^{-2} τ^{-1}), and northern China (-55.2 Wm^{-2} τ^{-1}). However, these values were less than estimates for the South Asian region (-89.4 Wm^{-2} τ^{-1}) where black carbon and organic carbon aerosols dominate [*Wang et al.*, 2007]. The values found in this study are more in line with those calculated for the Maldives [-72.2±5.5 Wm^{-2} τ^{-1}, *Bush and Valero*, 2002] and over the Indian Ocean [-75 Wm^{-2} τ^{-1}, *Ramanathan et al.*, 2001].

Aerosol loading not only changes radiative forcing in the earth-atmosphere system, but also alters the proportion of direct, global, and diffuse radiation at the surface. These results have implications in the study of the global carbon cycle [*Gu et al.*, 2002]. In eastern China, the mean direct shortwave flux reaching the surface in autumn to winter was reduced by about -68.5 $W{\cdot}m^{-2}$ and diffuse shortwave fluxes were enhanced by 42.5 $W{\cdot}m^{-2}$ in the presence of aerosols [*Liu et al.*, 2012]. Similar results were obtained in the PRD region, but the radiative forcing was stronger due to the presence of strongly absorbing aerosols (Fig. 7). During the dry season of the PRD region, global and direct radiative fluxes at the surface decreased by -37.50±9.43 and

-81.89±18.42 W·m^{-2}, respectively, and diffuse shortwave fluxes increased by 44.38±9.49 W·m^{-2}.

4. Conclusions

Aerosol optical and radiative properties, including frequency, temporal variability, classification and radiative forcing, have been analyzed using seven years of ground-based measurements made at Panyu, an observation site in the PRD region. The major conclusions are summarized as follows:

(1) In the dry season (October to the following February), aerosols in the PRD region were fine-mode, strongly absorbing particles, with annual mean values of AE and SSA equal to 1.33 and 0.87, respectively. The annual mean AOD at 550 nm was 0.535, which is relatively smaller in magnitude than AOD at 550 nm retrievals made at sites in eastern China.

(2) To sort out the major aerosol types and their radiative impacts in this region, AE and ω were used. Up to 90% of aerosols were dominated by fine-mode, strongly absorbing particles with mean AE = 1.35, ω = 0.14, and AOD = 0.52. The proportion of fine-mode, weakly absorbing particles was about 9.52%, with AE = 1.30, ω =0.04, and AOD = 0.65. Due to the minimal presence of dust in the PRD region, the aerosol coarse mode was negligible.

(3) Because of the strong absorption, the overall aerosol direct radiative effect is to significantly heat the atmosphere and cool the surface, and to alter the proportion of direct, global, and diffuse radiation at the surface. The annual mean shortwave direct radiation forcing at the surface, inside the atmosphere, and at the top of atmosphere was -33.51±8.41, 27.29±7.19,

and -6.22±2.22 W·m^{-2}, respectively. The annual mean reduction in global and direct radiation due to aerosols was -37.50±9.43 W·m^{-2} and -81.89±18.42 W·m^{-2}, respectively. The presence of aerosols caused 44.38±9.49 W·m^{-2} more diffuse radiation to reach the earth's surface.

(4) Given that aerosol radiative properties and forcing have not yet been well studied in the PRD region compared to the rest of China, these results can help constrain uncertainties in estimating regional anthropogenic aerosol radiative forcing. In future work, we will pay more attention on the properties of carbonaceous aerosols in the PRD region and their impacts on regional climate change.

Acknowledgements

This research work is funded by the National Natural Science Foundation of China (41175117, 40875090, 41373116), the MOST 973 Program (2013CB955804), the National "973" Program (2011CB403400), the Natural Science Foundation of Guangdong Province (S2012010008749), the National Natural Science Foundation of China and Guangdong Province Joint Fund (U1201232), the Special Research Project of Public Service Sectors (Weather) (GYHY201306042) and the Science and Technology Sponsorship Program of Guangdong Province (2010A030200012). The availability of the data used for this study is fully described in section 2 of this paper. The MODIS data were downloaded from the NASA Goddard Space Flight Center. we also thank SKYRAD.pack and SBDART model. The constructive suggestions from the anonymous reviewers are greatly appreciated.

References

Alam, K., T. Trautmann, and T. Blaschke (2011), Aerosol optical properties and radiative forcing over mega-city Karachi, *Atmos. Res., 101*, 773–782.

Andreae, M. O., O. Schmid, H. Yang, et al. (2008), Optical properties and chemical composition of the atmospheric aerosol in urban Guangzhou, China, *Atmos. Environ.*, *42*, 6335 – 6350.

Bush, B. C., and F. P. J. Valero (2002), Spectral aerosol radiative forcing at the surface during the Indian Ocean Experiment (INDOEX), *J. Geophys. Res.*, *107*(D19), doi:10.1029 /2000 JD000020.

Cao, J. J., S. C. Lee, K. F. Ho, et al. (2003), Characteristics of carbonaceous aerosol in Pearl River Delta Region, China during 2001 winter period, *Atmos. Environ.*, *37*, 1451–1460, doi:10.1016/S1352-2310(02)01002-6.

Cao, J. J., S. C. Lee, K. F. Ho, et al. (2004), Spatial and seasonal variation of atmospheric organic carbon and elemental carbon in Pearl River Delta region, China, *Atmos. Environ.*, *38*, 4447–4456. doi:10.1016/j.atmosenv.2004.05.016.

Chameides, W. L., et al. (1999), Case study of the effects of atmospheric aerosols and regional haze on agriculture: An opportunity to enhance crop yields in China through emission controls?, *Proc. Natl. Acad. Sci. U. S. A.*, *96*, 13,626– 13,633.

Che, H., G. Shi, A. Uchiyama, A. Yamazaki, H. Chen, P. Goloub, and X. Zhang (2008), Intercomparison between aerosol optical properties by a PREDE skyradiometer and CIMEL sunphotometer over Beijing, China, *Atmos. Chem. Phys.*, *8*, 3199–3214, doi:10.5194/acp-8-3199-2008.

Che, H., X. Zhang, H. Chen, B. Damiri, P. Goloub, Z. Li, X. Zhang, Y. Wei, H. Zhou, F. Dong, D. Li, and T. Zhou (2009) Instrument calibration and aerosol optical depth validation of the China Aerosol Remote Sensing Network, *J. Geophys. Res.*, *114*, D03206, doi:10.1029/2008JD011030.

Che, H., X. Xia, J. Zhu, et al. (2014), Column aerosol optical properties and aerosol radiative forcing during a serious haze-fog month over North China Plain in 2013 based on ground-based sunphotometer measurements, *Atmos. Phys.*, *14*, 2125–2138.

Cheng, Y. F., A.Wiedensohler, H. Eichler, et al. (2008), Aerosol optical properties and related chemical apportionment at Xinken in Pearl River Delta of China, *Atmos. Environ.,* *42*, 6351–6372, doi:10.1016/j.atmosenv.2008.02.034.

Choi, J. O., and C. E. Chung (2014), Sensitivity of aerosol direct radiative forcing to aerosol vertical Profile, *Tellus* B, *6*6, 24376,http://dx.doi.org/10.3402/tellusb.v66.24376.

Clarke, A., and V. Kapustin (2010), Hemispheric aerosol vertical profiles: Anthropogenic impacts on optical depth and cloud nuclei, *Science*, *329*, 1488–1492, doi:10.1126/science.1188838.

Corrigan, C. E., V. Ramanathan, and J. J. Schauer (2006), Impact of monsoon transitions on the physical and optical properties of aerosols, *J. Geophys. Res.*, *111*, D18208, doi:10.1029 /2005JD006370.

Deng, X., D. Wu, X. Tie, et al. (2006), Study on the effect of atmospheric aerosol on actinic flux and ozone in large city. Part I: Current research state abroad and at home and observed event, *Guangdong Meteorology*, *3*, 10-17. (In Chinese)

Deng, X., X. Zhou, D. Wu., et al. (2011), Effect of atmospheric aerosol on surface ozone variation over the Pearl River Delta region, *Sci China Earth Sci*., *54*, 744–752, doi:10.1007/s11430-011-4172-7.

Eck, T. F., B. N. Holben, J. S. Reid, O. Dubovik, A. Smirnov, N. T. O'Neill, I. Slutsker, and S. Kinne (1999), Wavelength dependence of the optical depth of biomass burning, urban, and desert dust aerosols, *J. Geophys. Res.*, *104*, 31,333-331,349.

Eck, T. F., et al. (2005), Columnar aerosol optical properties at AERONET sites in central eastern Asia and aerosol transport to the tropical mid-Pacific, *J. Geophys. Res.*, *110*, D06202, doi:10.1029/2004JD005274.

Gobbi, G. P., Y. J. Kaufman, I. Koren, and T. F Eck (2007), Classification of aerosol properties derived from AERONET direct sun data, *Atmos. Chem. Phys.*, *7*, 453–458, doi:10.5194/acp-7-453-2007.

Gu, L., D. Baldocchi, S. B. Verma, T. A. Black, T. Vesala, E. M. Falge, and P. R. Dowty (2002), Advantages of diffuse radiation for terrestrial ecosystem productivity, *J. Geophys. Res.*, *107*(D6), doi:10.1029/ 2001JD001242.

Guan, H., B. Schmid, A. Bucholtz, and R. Bergstrom (2010), Sensitivity of shortwave radiative flux density, forcing, and heating rate to the aerosol vertical profile, *J. Geophys. Res.*, *115*, D06209, doi:10.1029/2009JD012907.

Halthore, R. N., et al. (2005), Intercomparison of shortwave radiative transfer codes and Measurements, *J. Geophys. Res.*, *110*, D11206, doi:10.1029/2004JD005293.

Holben, B. N., et al. (1998), AERONET-A federated instrument network and data archive for aerosol characterization, *Remote Sens. Environ.*, *66*, 1–16.

Intergovernmental Panel on Climate Change (IPCC) (2007), Climate Change 2007: The Physical Science Basis. Contribution of Working Group I to the Fourth Assessment Report of the Intergovernmental Panel on Climate Change, edited by S. Solomon, D. Qin, and M. Manning, Cambridge Univ. Press, Cambridge, U. K.

Kaufman, Y. J., D. Tanré, and O. Boucher (2002a), A satellite view of aerosols in the climate System, *Nature*, *419*, 215 – 223, doi:10.1038/nature01091.

Kaufman, Y. J., J. V. Martins, L. A. Remer, M. R. Schoeberl, and M. A.Yamasoe (2002b), Satellite retrieval of aerosol absorption over the oceans using sunglint, *Geophys. Res. Lett.*, *29*(19), doi:10.1029/ 2002GL015403.

Kim, D.-H., B.-J. Sohn, T. Nakajima, and T. Takamura (2005), Aerosol radiative forcing over East Asia determined from ground-based solar radiation measurements, *J. Geophys. Res.*, *110*, D10S22, doi:10.1029/2004JD004678.

Khatri, P., T. Takamura, A. Shimizu, and N. Sugimoto (2014), Observation of low single scattering albedo of aerosols in the downwind of the East Asian desert and urban areas during the inflow of dust aerosols, *J. Geophys. Res. Atmos.*, *119*, 787–802, doi:10.1002/2013JD019961.

Kosmopoulos, P. G., D. G. Kaskaoutis, P. T. Nastos, H. D. Kambezidis (2008), Seasonal variation of columnar aerosol optical properties over Athens, Greece, based on MODIS data, *Remote. Sens. Environ., 112*, 2354–2366.

Kotchenruther, R. A., and P. V. Hobbs (1998), Humidification factors of aerosols from biomass burning in Brazil, *J. Geophys. Res.*, *103*, 32,081–32,089.

Lee, K. H., Z. Li, M. S. Wong, J. Xin, Y. Wang, W. M. Hao, and F. Zhao (2007), Aerosol single scattering albedo estimated across China from a combination of ground and satellite measurements, *J. Geophys. Res.*, *112*, D22S15, doi:10.1029/2007JD009077.

Lee, S., G. Bae, Y. Lee, et al. (2010), Correlation between light intensity and ozone formation for photochemical smog in urban air of Seoul, *Aerosol Air Qual. Res., 10*, 540-549.

Li, Z., et al. (2007), Aerosol optical properties and their radiative effects in northern China, *J. Geophys. Res., 112*, D22S01, doi:10.1029/2006JD007382.

Li, Z., X. Zhao, R. Kahn, et al. (2009), Uncertainties in satellite remote sensing of aerosols and impact on monitoring its long-term trend: a review and perspective,. *Ann. Geophys.*, *27*, 2755–2770.

Li, Z., K. H. Lee, Y. Wang, J. Xin, and W. M. Hao (2010), First observation‐based estimates of cloud−free aerosol radiative forcing across China, *J. Geophys. Res., 115*, D00K18, doi:10.1029/2009JD013306.

Liu, J., X. Xia, P. Wang, Z. Li, Y. Zheng, M. Cribb, and H. Chen (2007), Significant aerosol direct radiative effects during a pollution episode in northern China, *Geophys. Res. Lett.*, *34*, L23808,doi:10.1029/2007GL030953.

Liu, J., Y. Zheng, Z. Li, and R. Wu (2008), Ground-based remote sensing of aerosol optical properties in one city in northwest China, *Atmos. Res.*, *89*(1–2), 194–205.

Liu, J., Y. Zheng, Z. Li, C. Flynn, and M. Cribb (2012), Seasonal variations of aerosol optical properties, vertical distribution and associated radiative effects in the Yangtze Delta region of China, *J. Geophys. Res.*, *117*, D00K38, doi:10.1029/2011JD016490.

Liu, X., W. Zhang, M. Huang, et al. (2009), Effect of illumination intensity and light application time on secondary organic aerosol formation from the photooxidation of α-pinene, *J. Environ. Sci.*, *21*,447-451.

Logan, T., B. Xi, X. Dong, et al. (2013), Classification and investigation of Asian aerosol absorptive Properties, *Atmos. Chem. Phys.*, *13*, 2253–2265.

Myhre, G., D. Shindell, F.-M. Bréon, W. Collins, J. Fuglestvedt, and co-authors (2013), Anthropogenic and natural radiative forcing. In: Climate Change 2013: The Physical Science Basis. Contribution of Working Group I to the Fifth Assessment Report of the Intergovernmental Panel on Climate Change (eds. T. F. Stocker, D. Qin, G.-K. Plattner, M. Tignor, S. K. Allen, J. Boschung and co-authors.), Cambridge University Press, Cambridge, United Kingdom, pp. 659-740.

Nakajima, T., G. Tonna, R. Rao, et al. (1996), Use of sky brightness measurements from ground for remote sensing of particulate polydispersions, *Appl. Optics*, *35*(15), 2672-2686.

Pathak, B., G. Kalita, K. Bhuyan, P. K. Bhuyan, and K. K. Moorthy (2010), Aerosol temporal characteristics and its impact on shortwave radiative forcing at a location in the northeast of India, *J. Geophys. Res.*, *115*, D19204, doi:10.1029/2009JD013462.

Ramanathan, V., et al. (2001), Indian Ocean Experiment: An integrated analysis of the climate forcing and effects of the great Indo-Asian haze, *J. Geophys. Res.*, *106*, 28,371–28,398, doi:10.1029/2001JD900133.

Ricchiazzi, P., S. Yang, C. Gautier, and D. Sowle (1998), SBDART: A research and teaching software tool for plane-parallel radiative transfer in the Earth's atmosphere, *Bull. Am. Meteorol. Soc.*, *79*, 2101– 2114.

Rosenfeld, D., U. Lohmann, G. B. Raga, C. D. O'Dowd, M. Kulmala, S. Fuzzi, A. Reissell, M. O. Andreae (2008), Flood or drought: How do aerosols affect precipitation?, *Science*, *321*, 1309–1313, doi:10.1126/science.1160606.

Smirnov, A., B. N. Holben, T. F. Eck, O. Dubovik, and I. Slutsker (2000), Cloud screening and quality control algorithms for the AERONET database, *Remote Sens. Environ.*, *73*, 337–349.

Tao, R., H. Che, Q. Chen, Y. Wang, J. Sun, X. Zhang, S. Lu, J. Guo, H. Wang, and X. Zhang (2014), Development of an integrating sphere calibration method for Cimel sunphotometers in China aerosol remote sensing network, *Particuology*,*13*, 88-99.

Valenzuela, A., F. J. Olmo, H. Lyamani, M. Antón, A. Quirantes, and L. Alados-Arboledas (2012), Classification of aerosol radiative properties during African desert dust intrusions over southeastern Spain by sector origins and cluster analysis, *J. Geophys. Res.*, *117*, D06214, doi:10.1029/2011JD016885.

Wang, M. (1999), Atmospheric Chemistry (in Chinese), Chin. Meteorol. Press, Beijing.

Wang, S. H., N. H. Lin, M. D. Chou, and J. H. Woo (2007), Estimate of radiative forcing of Asian biomass-burning aerosols during the period of TRACE-P, *J. Geophys. Res.*, *112*, D10222, doi:10.1029/ 2006JD007564.

Wang, X., X. Ding, X. Fu., et al. (2012), Aerosol scattering coefficients and major chemical compositions of fine particles observed at a rural site in the central Pearl River Delta, South

China, *J. Environ. Sci.*, *24*(1), 72-77.

Wang, Z., D. Liu, Z. Wang, Y. Wang, P. Khatri, J. Zhou, T. Takamura, and G. Shi (2014), Seasonal characteristics of aerosol optical properties at the SKYNET Hefei site (31.90°N, 117.17°E) from 2007 to 2013, *J. Geophys. Res. Atmos.*, *119*, 6128–6139, doi:10.1002/2014JD021500.

Wu, D., G. Liao, X. Deng., et al. (2008), Transport condition of surface layer under haze weather over the Pearl River Delta, *J. Appl. Meteor. Sci.*, *19*(1), 1-9. (In Chinese)

Wu, D., J. Mao, X. Deng., et al. (2009), Black carbon aerosols and their radiative properties in the Pearl River Delta region, *Sci China Ser D-Earth Sci*, *52*(8), 1152-1163, doi: 10.1007/s11430-009-0115-y.

Xia, X., Z. Li, B. Holben, P. Wang, T. Eck, H. Chen, M. Cribb, and Y. Zhao (2007a), Aerosol optical properties and radiative effects in the Yangtze Delta region of China, *J. Geophys. Res.*, *112*, D22S12, doi:10.1029/2007JD008859.

Xia, X., H. Chen, P. Goloub, W. Zhang, B. Chatenet, and P. Wang (2007b), A compilation of aerosol optical properties and calculation of direct radiative forcing over an urban region in northern China, *J. Geophys. Res.*, *112*, D12203, doi:10.1029/2006JD008119.

Xia, X., H. Chen, Z. Li, P. Wang, and J. Wang (2007c), Significant reduction of surface solar irradiance induced by aerosols in a suburban region in northeastern China, *J. Geophys. Res.*, *112*, D22S02, doi:10.1029/2006JD007562.

Xia, X., Z. Li, P. Wang, H. Chen, and M. Cribb (2007d), Estimation of aerosol effects on surface irradiance based on measurements and radiative transfer model simulations in northern China, *J. Geophys. Res.*, *112*, D22S10, doi:10.1029/2006JD008337.

Xin, J., L. Wang, Y. Wang, Z. Li, and P. Wang (2011),Trends in aerosol optical properties over the Bohai Rim in Northeast China from 2004 to 2010, *Atmos. Environ.*, *45*, 6317-6325.

Yang, S., G. Y. Shi, B. Wang., et al. (2011), The application of AOD's spectral curve parameter to judgment of aerosol particle size, *J. Appl. Meteorol. Sci.*, *22*(2), 152−157. (In Chinese)

Yu, H., et al. (2006), A review of measurement-based assessments of aerosol direct radiative effect and forcing, *Atmos. Chem. Phys.*, *6*, 613–666, doi:10.5194/ acp-6-613-2006.

Yu, H., et al. (2009), Remote sensing and in-situ measurements of aerosol properties, burdens, and radiative forcing, in Atmospheric Aerosol Properties and Climate Impacts: Synthesis and Assessment Product 2.3: Report by the U.S. Climate Change Science Program and the Subcommittee on Global Change Research, edited by M. Chi, R. A. Kahn, and S. E. Schwartz, pp. 21–54, U.S. Clim. Change Sci. Program, Washington, D. C.

Zhao, F., and Z. Li (2007), Estimation of aerosol single - scattering albedo from solar direct spectral radiance and total broadband irradiances measured in China, *J. Geophys. Res.*, *112*, D22S03, doi:10.1029/ 2006JD007384.

Zheng, M., F. Wang, G. S. W. Hagler., et al. (2011), Sources of excess urban carbonaceous aerosol in the Pearl River Delta Region, *Atmos. Environ., 45*, 1175-1182.

Zhu, J., H. Che, X. Xia, H. Chen, P. Goloub, and W. Zhang (2014), Column-integrated aerosol optical and physical properties at a regional background atmosphere in North China Plain, *Atmos. Environ.*, *84*, 54-64.

Tables

Table 1. Number of days in each month with inversion data (AOD, SSA, and AE) available and the total number of data points in each month.

Year	Number of days					Year	Number of instantaneous data				
	Oct	Nov	Dec	Jan	Feb		Oct	Nov	Dec	Jan	Feb
2006	4	12	23	0	0	2006	24	64	102	0	0
2007	18	10	18	15	0	2007	47	57	67	73	0
2008	0	0	0	11	11	2008	0	0	0	54	32
2009	0	0	0	23	8	2009	0	0	0	169	42
2010	10	25	18	0	0	2010	38	119	105	0	0
2011	0	7	20	14	10	2011	0	33	99	51	26
2012	0	0	0	4	2	2012	0	0	0	10	7

Figures

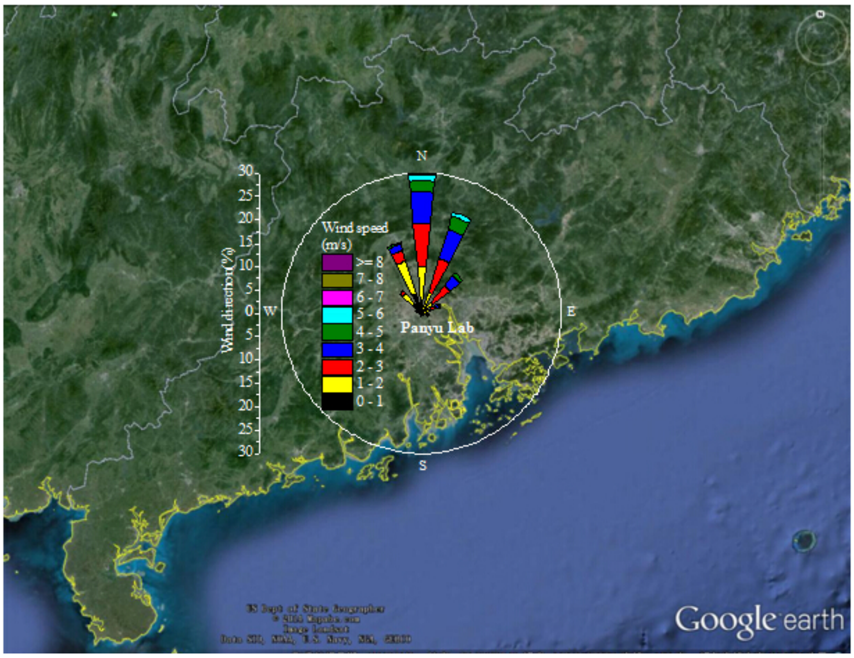

Fig. 1. Location of Panyu, the observation site in the PRD region. Mean hourly wind speeds and directions at the site are shown in the wind rose map.

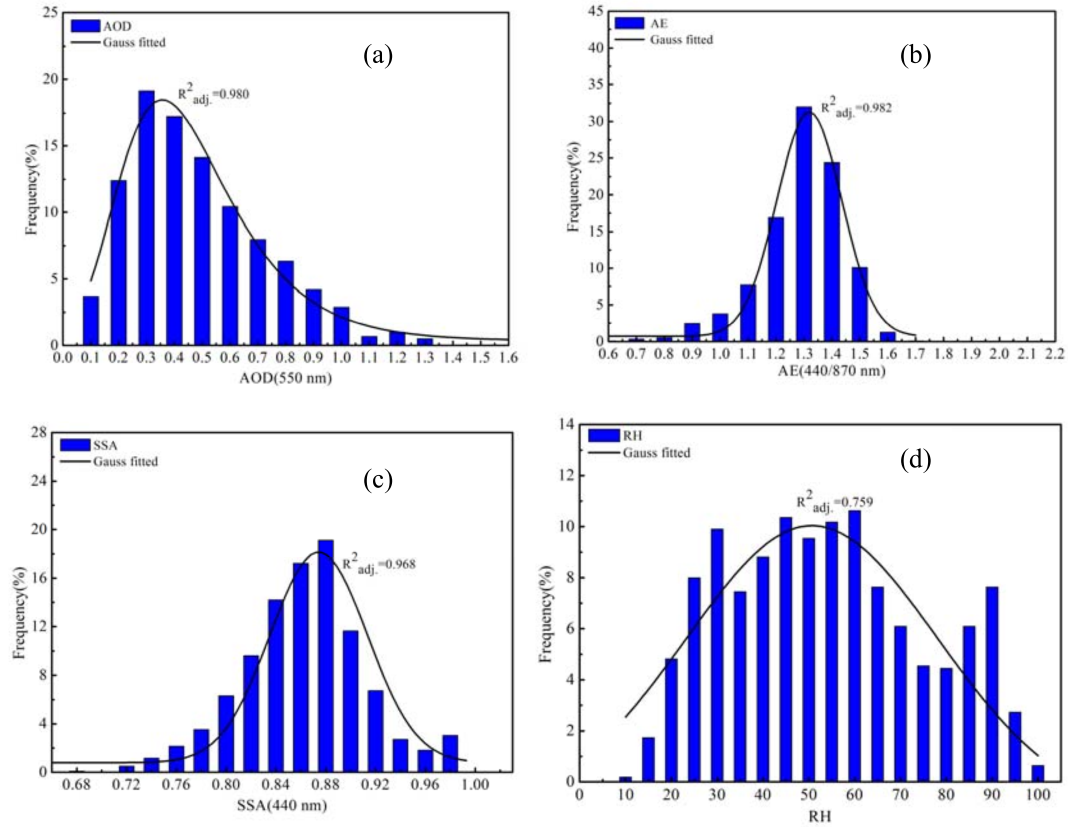

Fig. 2. Frequency distributions of (a) AOD at 550 nm, (b) the 440-870 nm AE, (c) SSA at 440 nm, and (d) RH for the PRD region. The black curve represents the Gaussian distribution.

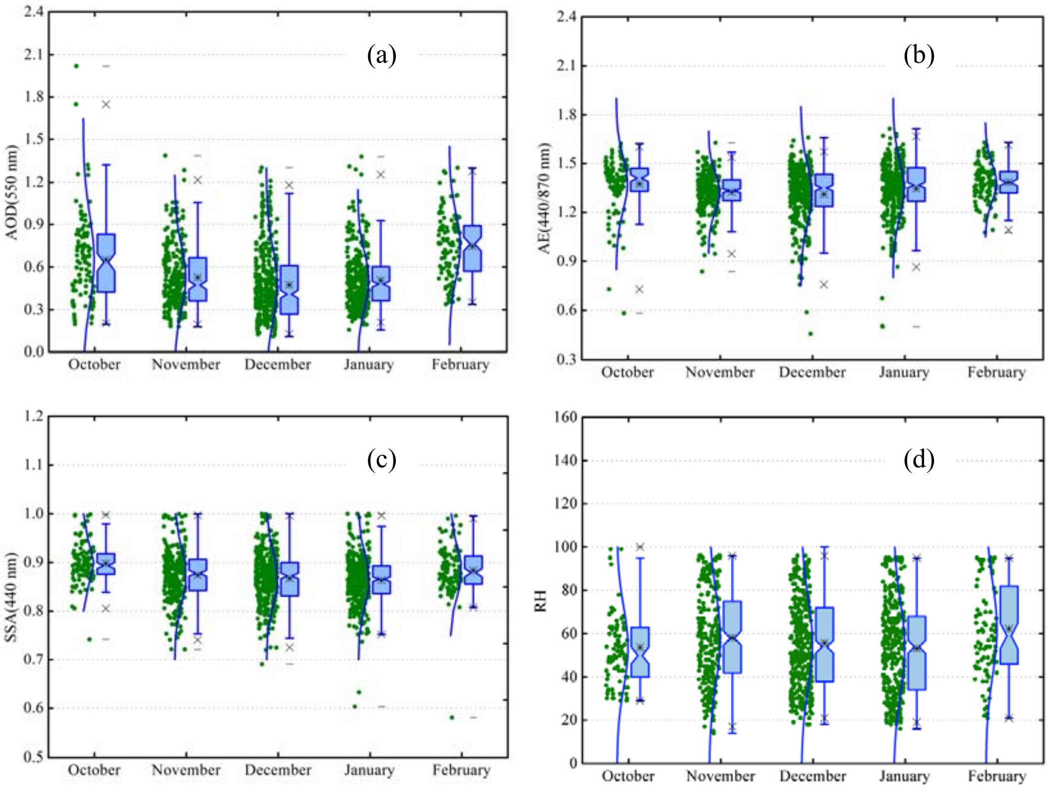

Fig. 3. Monthly distributions (green dots) of (a) AOD at 550 nm, (b) the 440-870 nm AE, (c) SSA at 440 nm, and (d) RH over the PRD region. The blue curves through the green dots represent Gaussian distributions. The notches in the notched box whisker plots represent the 95% confidence levels of the median values. Non-overlapping notches indicate that the medians are significantly different from each other.

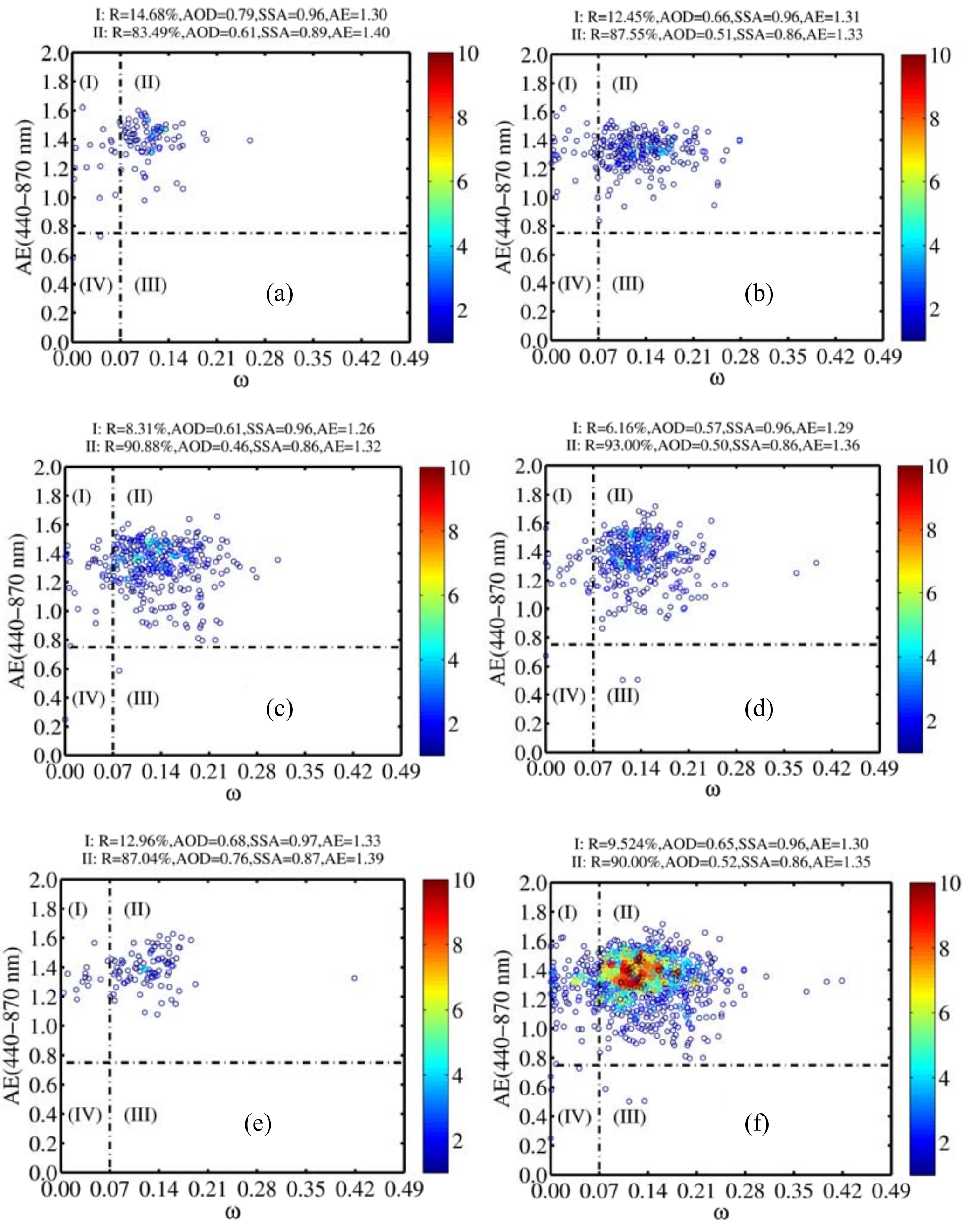

Fig. 4. Classification of the mean physico-chemical properties of aerosols into four regions using AE and ω at 440 nm. The color scale represents the relative density of points. Panels (a) - (f) correspond to October, November, December, January, February, and total data, respectively, of the years 2006-2012.

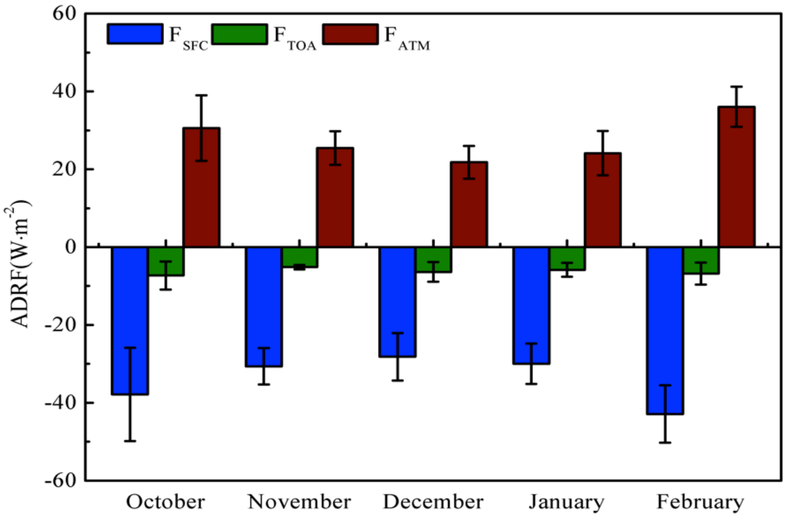

Fig. 5. Monthly mean diurnal aerosol direct radiative forcing (ADRF) at the surface (F_{SFC}), at the top of the atmosphere (F_{TOA}), and within the atmosphere (F_{ATM}).

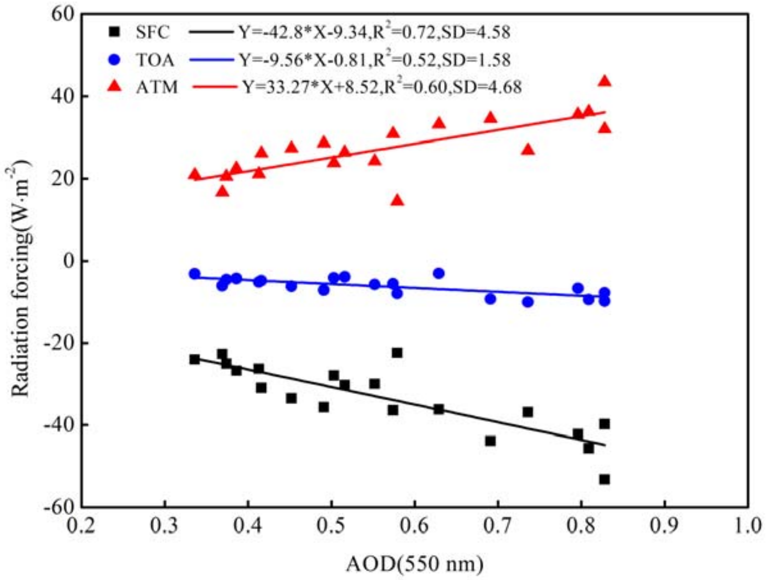

Fig. 6. Diurnal ADRF at the surface (SRF, black), top of the atmosphere (TOA, blue), and within the atmosphere (ATM, red) as a function of AOD at 550 nm over the PRD region. Best-fit lines through the points are shown and linear regression functions and statistics (coefficient of determination, R^2, and standard deviation, SD) are given.

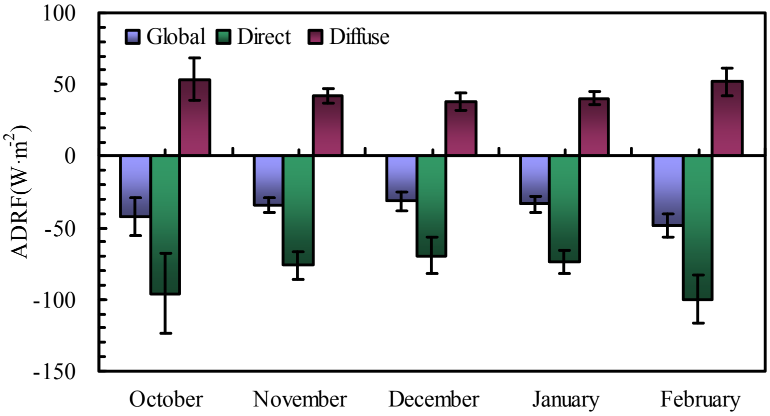

Fig. 7. Aerosol-induced monthly variations in surface downwelling global, direct, and diffuse shortwave irradiances.